POLISH MARITIME RESEARCH 3 (119) 2023 Vol. 30; pp. 119-131
10.2478/pomr-2023-0045

EVENT-TRIGGERED ADAPTIVE NEURAL NETWORK TRAJECTORY TRACKING CONTROL FOR UNDERACTUATED SHIPS UNDER UNCERTAIN DISTURBANCE

Wenxue Su*
Qiang Zhang
School of Navigation and shipping, Shandong Jiaotong University, China
Yufeng Liu
University of Toronto OISE, China

Corresponding author: *71837989@qq.com (Wenxue Su)*

ABSTRACT

An adaptive neural network (NN) event-triggered trajectory tracking control scheme based on finite time convergence is proposed to address the problem of trajectory tracking control of underdriven surface ships. In this scheme, both NNs and minimum learning parameters (MLPS) are applied. The internal and external uncertainties are approximated by NNs. To reduce the computational complexity, MLPs are used in the proposed controller. An event-triggered technique is then incorporated into the control design to synthesise an adaptive NN-based event-triggered controller with finite-time convergence. Lyapunov theory is applied to prove that all signals are bounded in the tracking system of underactuated vessels, and to show that Zeno behavior can be avoided. The validity of this control scheme is determined based on simulation results, and comparisons with some alternative schemes are presented.

Keywords: Keywords: event-triggered control; underactuated marine surface vessels; adaptive neural network; trajectory tracking; finite-time

INTRODUCTION

Since the 20th century, surface transport via marine shipping has received unprecedented amounts of research attention [1][2]. The use of intelligent ships, for example based on artificial intelligence and digital twins, is an important development in the area of ocean transportation, and motion control of such ships is an essential aspect of achieving intelligent operation [3][4]. Trajectory tracking control for ships is an influential line of research in the domain of ship motion control, and the issue of how to achieve fast, high-precision tracking has always been one of the main focuses in this field [5].

However, the shipping itself is characterised by high inertia, long time lags, and nonlinearity. In addition, there are various other factors that affect the internal dynamic uncertainties and cause external disturbances, thereby creating great difficulties for high-precision trajectory tracking control. To solve these problems, control algorithms such as neural networks (NNs) [6]-[9], fuzzy methods [10]-[14], sliding modes [15]-[17], and adaptive backstepping [18]-[20] have been developed, and many of these have been applied to achieve trajectory tracking control of ships. Control schemes based on these algorithms have solved the problems described above to a certain extent, but can only obtain asymptotically stable results when the system time tends to infinity.

Achieving high-precision tracking control of ships within a limited time can solve a series of engineering problems. For example, when a ship is operating in a complex environment and detects other ships or obstacles in the sea ahead, fast, high-precision tracking allows it to avoid these obstacles promptly, thereby improving the safety of operation. Research into finite-time trajectory tracking control in shipping therefore has many practical implications for engineering applications. In [21], a finite-time control scheme based on the sliding mode and adaptive theory was designed for the formation control of UAVs. In [22], a synergistic heading control strategy based on a hyperbolic tangent guidance method was designed to enable the ship to complete tracking control within a limited time. In [23], a composite perturbation was estimated by a finite-time perturbation observer; virtual control was also achieved using a finite-time command filter, and a control scheme was designed under full constraints. In [24], a finite time was applied to the problem of power positioning control, and when combined with a non-singular fast terminal sliding mode strategy, the convergence speed and immunity of the system were greatly improved.

Research into the finite-time control schemes mentioned above has greatly improved the convergence speeds of such systems. However, with the recent advances in control accuracy, a higher energy output is often required. In practical engineering terms, this will undoubtedly increase the wear and tear of the thruster and controller. To solve these problems, event-triggered (ET) techniques have begun to be applied to ship motion control. In [25], an ET control scheme with static trigger conditions was first developed. In [26], time-triggered control schemes with dynamic trigger conditions were developed to further extend the interaction time. In [27], ET control schemes with periodicity were investigated with the aim of relaxing the restrictions on the monitoring of trigger conditions. Following the introduction of stringent policies for energy reduction and environmental protection nationwide, applications involving event triggering for ship motion and control are also being developed [28][29].

Inspired by these research studies, this paper presents the design of an ET trajectory tracking control scheme based on finite-time convergence for underdriven ships with adaptive NNs. The main contributions of this study are as follows:

(1) Under conditions of dynamic uncertainty and external disturbance, a finite-time trajectory tracking control scheme is proposed that combines finite-time control theory, NNs, minimum learning parameters (MLPs), and depth information robust adaptive methods to achieve tracking control of underactuated ships within a finite time.
(2) The proposed finite-time trajectory tracking control scheme is combined with a fixed-threshold ET method to decrease the update frequency of the controller, reduce the losses of the actuator, and avoid Zeno behavior.

MATHEMATICAL MODELLING OF SHIP MOTION

A general mathematical model with three degrees of freedom for underdriven surface ship tracking control can be expressed in the following form [30]:

$$\begin{cases} \dot{x} = u\cos(\psi) - v\sin(\psi) \\ \dot{y} = u\sin(\psi) + v\cos(\psi) \\ \dot{\psi} = r \end{cases} \tag{1}$$

$$\begin{cases} \dot{u} = f_u(u,v,r) + \dfrac{1}{m_u}\left[\tau_u + d_u\right] \\ \dot{v} = f_v(u,v,r) + \dfrac{1}{m_v}d_v \\ \dot{r} = f_r(u,v,r) + \dfrac{1}{m_r}\left[\tau_r + d_r\right] \end{cases} \tag{2}$$

$$\begin{cases} f_u(u,v,r) = \dfrac{1}{m_u}(m_v vr - Y_r r^2 + X_u u + X_{u|u|}|u|u) \\ f_v(u,v,r) = \dfrac{1}{m_v}(Y_v v + Y_{|v|v}|v|v + Y_{|r|v}|r|v + Y_r r - m_u ur + Y_{|v|r}|v|r + Y_{|r|r}|r|r) \\ f_r(u,v,r) = \dfrac{1}{m_r}[(m_u - m_v)uv + Y_r ur + N_v v + N_r r + N_{|r|v}|r|v + N_{|v|v}|v|v + N_{|v|r}|v|r + N_{|r|r}|r|r] \end{cases} \tag{3}$$

In Eq. (3), x, y, ψ are the attitude variables of the ship's position coordinates and bow angle, respectively; u, v, r are the ship's velocity variables; d_u, d_v, d_r denote unmeasured, unknown disturbances; τ_u, τ_r are the input moments; and $f_u(u,v,r)$, $f_v(u,v,r)$, $f_r(u,v,r)$ are higher-order hydrodynamic terms.

Assumption 1: $f_i(u,v,r)$, m_i and $i = \{u,v,r\}$ are unknown, but their external disturbances d_i, $i = \{u,v,r\}$ are unknown and bounded; that is say, there exist unknown positive constants σ_u, σ_v, σ_r such that d_u, d_v, d_r satisfy $|d_u| \le \sigma_u$, $|d_v| \le \sigma_v$, $|d_r| \le \sigma_r$.

Definition: The nonlinear control system is described as in Eq. (4):

$$\dot{x} = f(x), x(0) = x_o, x \in \Omega_0 \subset R^n \tag{4}$$

where $x \in R^n$ is the state variable of the system, Ω_0 is a spherical domain containing the origin, and $f(x)$ is a continuous function. For arbitrary initial conditions x_0, the system in Eq. (4) can be said to be semi-globally stable within a finite time, in practice, if there exists a constant $\Im > 0$ and a settling time function $0 < T(\Im, x_o) < \infty$ such that $\|x(t)\| \le \Im$, $t \ge T(x_0)$ [31].

CONTROLLER DESIGN

The trajectory tracking control process is shown in Fig. 1.

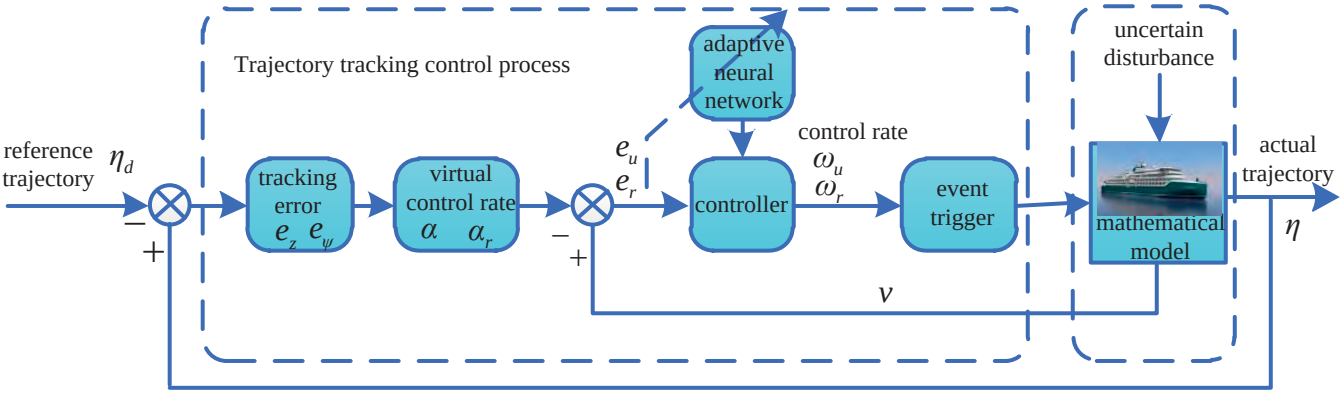

Fig. 1 Control flow diagram for trajectory tracking

To solve the problem of lateral drive mismatch of underdriven ships, a method from the existing literature [32] is used, and the following transformations are performed. First, we define the tracking error for an underdriven surface ship:

$$\begin{cases} e_x = x - x_d \\ e_y = y - y_d \\ e_\psi = \psi - \psi_d \end{cases} \tag{5}$$

where x_d, y_d, ψ_d represent the desired position and heading angle. A transformation of Eq. (5) yields

$$e_z = \begin{bmatrix} x - x_d \\ y - y_d \end{bmatrix} \tag{6}$$

From Eq. (6), we have

$$\dot{e}_z = u g_u(\psi) + v g_v(\psi) - \begin{pmatrix} \dot{x}_d \\ \dot{y}_d \end{pmatrix} \tag{7}$$

where $g_u(\psi) = \begin{bmatrix} \cos\psi \\ \sin\psi \end{bmatrix}$, $g_v(\psi) = \begin{bmatrix} -\sin\psi \\ \cos\psi \end{bmatrix}$.

To stabilise the tracking error e_z and e_ψ, we can construct the Lyapunov functions $V_1 = \frac{1}{2} e_z^T e_z + \frac{1}{2} \psi_e^2$. We can then design dummy control variables with the following form:

$$\begin{cases} \alpha = -k_{11} e_z - \dfrac{k_{12} e_z}{\sqrt{\|e_z\|^2 + \varsigma_z^2}} - v g_v(\psi) + \begin{pmatrix} \dot{x}_d \\ \dot{y}_d \end{pmatrix} \\ \alpha_r = -k_{31} e_\psi - \dfrac{k_{32} e_\psi}{\sqrt{\|e_\psi\|^2 + \varsigma_\psi^2}} + \dot{\psi}_d \end{cases} \tag{8}$$

The desired forward velocity, turning bow angular velocity and heading angle are expressed as shown in Eq. (9):

$$\begin{cases} u_d = \alpha_u = \|\alpha\| \\ r_d = \alpha_r = -k_{31} e_\psi - \dfrac{k_{32} e_\psi}{\sqrt{\|e_\psi\|^2 + \varsigma_\psi^2}} + \dot{\psi}_d \\ \psi_d = \arctan(\alpha_y, \alpha_x) \end{cases} \tag{9}$$

where ψ_d is obtained from $u_d = \alpha_u = \|\alpha\|$ inverse solution, and α_x, α_y are the virtual control rates of the position coordinates.

We define the error variables for the velocities as:

$$\begin{cases} e_u = u - \alpha_u \\ e_r = r - \alpha_r \end{cases} \tag{10}$$

From Eq. (10), we obtain

$$\begin{cases} \dot{e}_u = f_u(u,v,r) + \dfrac{1}{m_u}\left(\tau_u + d_u\right) - \dot{\alpha}_u \\ \dot{e}_r = f_r(u,v,r) + \dfrac{1}{m_r}\left(\tau_r + d_r\right) - \dot{\alpha}_r \end{cases} \tag{11}$$

Lemma 1: For any given continuous smooth function defined on a compact set $\Omega \subset R^n$ [33][34], we have

$$h(x) = W^{*T} s(x) + \varepsilon, \forall x \in \Omega \tag{12}$$

where ε is the approximation error, and for all $x \in \Omega$, there is a vector $\varepsilon^* > 0$ that satisfies $|\varepsilon| \le \varepsilon^*$; W^* is the weight vector under ideal conditions, and $s(x)$ is the central function. In general, the vector of ideal NN weights is unknown, and needs to be estimated. This problem can be interpreted as minimising $|\varepsilon|$ on $x \in \Omega \subset R^n$ to W, i.e.,

$$W^* = \arg\min_{W \in R^l} \left\{ \sup_{x \in \Omega} \left| h(x) - W^{\mathrm{T}} s(x) \right| \right\} \tag{13}$$

Assumption 2: In the compact set $\Omega_x \subset R^n$, the RBF neural network W^* used to approximate the unknown vector has bounded weights; that is, $\|W^*\| \le W_M$, W_M is a positive constant.

Due to the unknown dynamic uncertainties of $f_u(u,v,r)$ and $f_r(u,v,r)$, they cannot be used in the design of the controller. We therefore use RBF NNs to approximate $f_u(u,v,r)$ and $f_r(u,v,r)$, as follows:

$$\begin{cases} f_u(u,v,r) = W_u^{\,T} \sigma_u(\eta) + \varepsilon_u \\ f_r(u,v,r) = W_r^{\,T} \sigma_r(\eta) + \varepsilon_r \end{cases} \tag{14}$$

where W_u and W_r are the matrices of NN weights; $\sigma_u(\eta)$ and $\sigma_r(\eta)$ are functions of the NN; and ε_u, ε_r are the approximation errors. The expressions in Eq. (14) are then substituted into Eq. (11) to give

$$\begin{cases} \dot{e}_u = W_u^{\,T} \sigma_u(\eta) + \varepsilon_u + \dfrac{1}{m_u}\left(\tau_u + d_u\right) - \dot{\alpha}_u \\ \dot{e}_r = W_r^{\,T} \sigma_r(\eta) + \varepsilon_r + \dfrac{1}{m_r}\left(\tau_r + d_r\right) - \dot{\alpha}_r \end{cases} \tag{15}$$

Combined with a design concept based on the robust adaptive depth information method and using RBFNNs and MLPs, the following expressions can be obtained:

$$\begin{cases} \left\| W_u^{\,T} \sigma_u(\eta) + \varepsilon_u + \dfrac{d_u}{m_u} \right\| \le \left\| W_u^{\,T} \right\| \left\| \sigma_u(\eta) \right\| + \left| \varepsilon_u + \dfrac{d_u}{m_u} \right| \\ \qquad = \Theta_u \zeta_u(Z) \\ \left\| W_r^{\,T} \sigma_r(\eta) + \varepsilon_r + \dfrac{d_r}{m_r} \right\| \le \left\| W_r^{\,T} \right\| \left\| \sigma_r(\eta) \right\| + \left| \varepsilon_r + \dfrac{d_r}{m_r} \right| \\ \qquad = \Theta_r \zeta_r(Z) \end{cases} \tag{16}$$

where $\begin{cases} \Theta_u = \max\left\{ \left\| W_u^{\,T} \right\|, \left| \varepsilon_u + \dfrac{d_u}{m_u} \right| \right\} \\ \Theta_r = \max\left\{ \left\| W_r^{\,T} \right\|, \left| \varepsilon_r + \dfrac{d_r}{m_r} \right| \right\} \end{cases} \begin{cases} \zeta_u(Z) = \left\| \sigma_u(\eta) \right\| + 1 \\ \zeta_r(Z) = \left\| \sigma_r(\eta) \right\| + 1 \end{cases}$.

Through this transformation, the learning parameters of adaptive parameters are obviously reduced.

Based on this result, the Lyapunov function $V_2 = \frac{1}{2} u_e^{\,2} + \frac{1}{2} r_e^{\,2}$ is constructed and the following expressions for the control rate are designed:

$$\begin{cases} \omega_u(t) = m_u \left[-k_{21} e_u - \dfrac{k_{22} e_u}{\sqrt{\left\| e_u \right\|^2 + \zeta_u^{\,2}}} - c_1 e_u \hat{\Theta}_u \zeta_u^{\,2}(Z) + \dot{\alpha}_u \right] \\ \omega_r(t) = m_r \left[-k_{41} e_r - \dfrac{k_{42} e_r}{\sqrt{\left\| e_r \right\|^2 + \zeta_r^{\,2}}} - c_2 e_r \hat{\Theta}_r \zeta_r^{\,2}(Z) + \dot{\alpha}_r \right] \end{cases} \tag{17}$$

The adaptive rates are then as follows:

$$\begin{cases} \dot{\hat{\Theta}}_u = \acute{y}_1 \zeta_u^{\,2}(Z) \left\| e_u \right\|^2 - {}_1\Theta \\ \dot{\hat{\Theta}}_r = \acute{y}_2 \zeta_r^{\,2}(Z) \left\| e_r \right\|^2 - {}_2\Theta \end{cases} \tag{18}$$

where k_{11}, k_{12}, k_{21}, k_{22}, c_1, c_2, $\acute{y}_1$, $\acute{y}_2$ are design parameters with values greater than zero.

The measurement errors are defined as:

$$\begin{cases} e_{\xi_u}(t) = \omega_u(t) - \tau_u(t), \ t \in [t_k, t_{k+1}) \\ e_{\xi_r}(t) = \omega_r(t) - \tau_r(t), \ t \in [t_k, t_{k+1}) \end{cases} \tag{19}$$

where t is the trigger time interval; $\tau_u(t)$, $\tau_r(t)$ are the values for the controller at the previous departure time; and

$\tau_u(t)$, $\tau_r(t)$ are kept constant by the zero-order holder from the trigger time t_k until the trigger time is updated.

The event triggering conditions are designed as follows [35]:

$$\begin{cases} \tau_u(t) = \omega_u(t_k), \forall t \in [t_k, t_{k+1}) \\ t_{k+1} = \inf\left\{ t \in R \middle| e_{\xi_u}(t) \middle| \geq \eta_u \right\} \end{cases} \tag{20}$$

$$\begin{cases} \tau_r(t) = \omega_r(t_k), \forall t \in [t_k, t_{k+1}) \\ t_{k+1} = \inf\left\{ t \in R \middle| e_{\xi_r}(t) \middle| \geq \eta_r \right\} \end{cases} \tag{21}$$

where η_u and η_r are design parameters with values greater than zero. When the trigger condition is violated, the update time for the controller is marked as t_{k+1}, and the control signal for the controller is simultaneously updated to $\omega_u(t_{k+1})$ as the control input to the system.

STABILITY ANALYSIS

We select the following Lyapunov function for the control system:

$$V = V_1 + V_2 + \frac{1}{2g_u}\left(\Theta_u - g_u\hat{\Theta}_u\right)^2 + \frac{1}{2g_r}\left(\Theta_r - g_r\Theta_r\right)^2 \tag{22}$$

During the event trigger interval $[t_k, t_k + 1)$, since $\omega_i(t) - \tau_i(t) \leq m_i$, $i = u, r$. Hence, there is a continuous time-varying parameter $\Xi(t)$ that satisfies the conditions $\Xi(t_k) = 0$, $\Xi(t_{k+1}) = \pm 1$, $\Xi(t) \leq 1$, meaning that $\forall t \in [t_k, t_{k+1})$ is not difficult to obtain.

$$\begin{cases} \omega_u(t) = \tau_u(t) + \Xi_u(t)\eta_u \\ \omega_r(t) = \tau_r(t) + \Xi_r(t)\eta_r \end{cases} \tag{23}$$

If $\Delta_e = ug_u(\psi) - u^* g_u(\psi^*)$, according to Young's inequality, $e_z\Delta_e \leq \frac{e_z^2}{10} + \frac{5}{2}\|\Delta_e\|^2$ can be obtained. From the time derivative of Eq. (22), we can obtain expressions as follows:

$$\dot{V} \leq -e_z^T(k_{11} - 0.1)e_z - \frac{e_z^T k_{12} e_z}{\sqrt{\|e_z\|^2 + \varsigma_z^2}} + \frac{5}{2}\|\Delta_e\|^2 + e_u m_u^{-1}\tau_u + \|e_u\|\Theta_u\zeta_u(Z) \tag{24}$$
$$-\left(\Theta_u - g_u\hat{\Theta}_u\right)\dot{\Theta}_u - k_{31}e_\psi^2 - \frac{k_{32}e_\psi^2}{\sqrt{\|e_\psi\|^2 + \varsigma_\psi^2}} + e_r m_r^{-1}\tau_r + \|e_r\|\Theta_r\zeta_r(Z) - \left(\Theta_r - g_r\Theta_r\right)\dot{\Theta}_r$$

From Young's inequality $\lambda\gamma \leq \frac{1}{2}\lambda^2 + \frac{1}{2}\gamma^2$, we obtain

$$\dot{V} \leq -e_z^T(k_{11} - 0.1)e_z - \frac{e_z^T k_{12} e_z}{\sqrt{\|e_z\|^2 + \varsigma_z^2}} + \frac{5}{2}\|\Delta_e\|^2 - g_u\left(k_{21} + \frac{1}{2}\right)e_u^2$$
$$-\frac{g_u k_{22} e_u^2}{\sqrt{\|e_u\|^2 + \varsigma_u^2}} - c_1 g_u\hat{\Theta}_u\zeta_u^2(Z)e_u + \frac{1}{2}\|\Xi_u(t)m_u^{-1}\eta_u\|^2 + \|e_u\|\Theta_u\zeta_u(Z) \tag{25}$$
$$-\left(\Theta_u - g_u\hat{\Theta}_u\right)\dot{\Theta}_u - k_{31}e_\psi^2 - \frac{k_{32}e_\psi^2}{\sqrt{\|e_\psi\|^2 + \varsigma_\psi^2}} - g_r\left(k_{41} + \frac{1}{2}\right)e_r^2 - \frac{g_r k_{42} e_r^2}{\sqrt{\|e_r\|^2 + \varsigma_r^2}}$$
$$-c_2 g_r\hat{\Theta}_r\zeta_r^2(Z)e_r + \|e_r\|\Theta_r\zeta_r(Z) + \frac{1}{2}\|\Xi_r(t)m_r^{-1}\eta_r\|^2 - \left(\Theta_r - g_r\hat{\Theta}_r\right)\dot{\Theta}_r$$

Based on Young's inequality, the following expressions can be obtained:

$$\begin{cases} \|e_u\|\Theta_u\zeta_u(Z) \leq \Theta_u\|e_u\|^2\zeta_u^2(Z) + \dfrac{\Theta_u}{4c_1} \\ \|e_r\|\Theta_r\zeta_r(Z) \leq \Theta_r\|e_r\|^2\zeta_r^2(Z) + \dfrac{\Theta_r}{4c_2} \end{cases} \tag{26}$$

Eq. (26) is then substituted into Eq. (25) to give

$$\dot{V} \leq -e_z^T\kappa_{11}e_z - \frac{e_z^T\kappa_{12}e_z}{\sqrt{\|e_z\|^2 + \varsigma_z^2}} + \frac{5}{2}\|\Delta_e\|^2 - g_u\kappa_{21}e_u^2 - \frac{g_u\kappa_{22}e_u^2}{\sqrt{\|e_u\|^2 + \varsigma_u^2}} - \kappa_{11}e_\psi^2 \tag{27}$$
$$-\frac{\kappa_{11}e_\psi^2}{\sqrt{\|e_\psi\|^2 + \varsigma_\psi^2}} + \frac{1}{2}\|\Xi_u(t)m_u^{-1}\eta_u\|^2 - g_r\kappa_{21}e_r^2 - \frac{g_r\kappa_{22}e_r^2}{\sqrt{\|e_r\|^2 + \varsigma_r^2}} + \iota_1\left(\Theta_u - g_u\hat{\Theta}_u\right)\dot{\Theta}_u$$
$$+\iota_2\left(\Theta_r - g_r\hat{\Theta}_r\right)\dot{\Theta}_r + \frac{\Theta}{4c_1} + \frac{\Theta}{4c_2} + \frac{1}{2}\|\Xi_r(t)m_r^{-1}\eta_r\|^2$$

where $\kappa_{11} = \min\left\{(k_{11} - 0.1), k_{31}\right\}$, $\kappa_{21} = \min\left\{k_{21} + 0.5, k_{41} + 0.5\right\}$, $\kappa_{12} = \min\left\{k_{12}, k_{32}\right\}$, $\kappa_{22} = \min\left\{k_{22}, k_{42}\right\}$.

We use the following Young's inequality:

$$\begin{cases} \left(\Theta_u - g_u\hat{\Theta}_u\right)\Theta_u \leq -\dfrac{1}{2g_u}\left(\Theta_u - g_u\Theta_u\right)^2 + \dfrac{\Theta_u^2}{2g_u} \\ \left(\Theta_r - g_r\hat{\Theta}_r\right)\Theta_r \leq -\dfrac{1}{2g_r}\left(\Theta_r - g_r\Theta_r\right)^2 + \dfrac{\Theta_r^2}{2g_r} \end{cases} \tag{28}$$
$$\begin{cases} \dfrac{\iota_1}{2g_u}\left|\Theta_u - g_u\hat{\Theta}_u\right| \leq \dfrac{\iota_1}{4g_u}\left|\Theta_u - g\Theta_u\right|^2 + \dfrac{\iota_1}{4g_u} \\ \dfrac{\iota_2}{2g_r}\left|\Theta_r - g_r\hat{\Theta}_r\right| \leq \dfrac{\iota_2}{4g_r}\left|\Theta_r - g_r\Theta_r\right|^2 + \dfrac{\iota_2}{4g_r} \end{cases}$$

By adding or subtracting $\begin{cases} \frac{\iota_1}{2g_u}\left|\Theta_u - g_u\hat{\Theta}_u\right| \\ \frac{\iota_2}{2g_r}\left|\Theta_r - g_r\hat{\Theta}_r\right| \end{cases}$ to both sides of Eq. (27) and combining with Eq. (28), the following equation can be obtained:

$$\begin{aligned}\dot{V} \le & -e_z^{\ T}\kappa_{11}e_z - \frac{e_z^{\ T}\kappa_{12}e_z}{\sqrt{\|e_z\|^2+\varsigma_z^{\ 2}}} + \frac{5}{2}\|\Delta_e\|^2 - g_u\kappa_{21}e_u^{\ 2} - \frac{g_u\kappa_{22}e_u^{\ 2}}{\sqrt{\|e_u\|^2+\varsigma_u^{\ 2}}} - \kappa_{11}e_\psi^{\ 2} - \frac{\kappa_{11}e_\psi^{\ 2}}{\sqrt{\|e_\psi\|^2+\varsigma_\psi^{\ 2}}} \\ & - g_r\kappa_{21}e_r^{\ 2} - \frac{g_r\kappa_{22}e_r^{\ 2}}{\sqrt{\|e_r\|^2+\varsigma_r^{\ 2}}} - \frac{\iota_1}{4g_u}\left(\Theta_u - g_u\hat{\Theta}_u\right)^2 - \frac{\iota_2}{4g_r}\left(\Theta_r - g_r\Theta_r\right)^2 - \frac{\iota_1}{2g_u}\left|\Theta_u - g_u\Theta_u\right| \\ & - \frac{\iota_2}{2g_r}\left|\Theta_r - g_r\hat{\Theta}_r\right| + \frac{\iota_1}{4g_u} + \frac{\iota_2}{4g_r} + \frac{\iota_1\Theta_u^{\ 2}}{2g_u} + \frac{\iota_2\Theta_r^{\ 2}}{2g_r} + \frac{\Theta_u}{4c_1} + \frac{\Theta_r}{4c_2} + \frac{1}{2}\left\|\Xi_u(t)m_u^{-1}\eta_u\right\|^2 + \frac{1}{2}\left\|\Xi_r(t)m_r^{-1}\eta_u\right\|^2\end{aligned} \tag{29}$$

Lemma 2: For any constant $\varsigma > 0$ and any scalar $\upsilon \in R$, the inequality in Eq. (30) holds [36]:

$$0 \le |\upsilon| - \frac{\upsilon^2}{\sqrt{\upsilon^2+\varsigma^2}} < \varsigma \tag{30}$$

From Lemma 2, we obtain

$$\begin{cases} -\frac{e_z^{\ T}\kappa_{12}e_z}{\sqrt{\|e_z\|^2+\varsigma_z^{\ 2}}} < \kappa_{12}\left(\varsigma_z - \|e_z\|\right) \\ -\frac{g_u\kappa_{22}e_u^{\ 2}}{\sqrt{\|e_u\|^2+\varsigma_u^{\ 2}}} < \kappa_{22}\left[g_u\left(\varsigma_u - \|e_u\|\right)\right] \end{cases} \tag{31}$$

$$\begin{cases} -\frac{\kappa_{12}e_\psi^{\ 2}}{\sqrt{\|e_\psi\|^2+\varsigma_\psi^{\ 2}}} < \kappa_{12}\left(\varsigma_\psi - \|e_\psi\|\right) \\ -\frac{g_r\kappa_{22}e_r^{\ 2}}{\sqrt{\|e_r\|^2+\varsigma_r^{\ 2}}} < \kappa_{22}\left[g_r\left(\varsigma_r - \|e_r\|\right)\right] \end{cases}$$

Eq. (32) is substituted into Eq. (29).

$$\begin{aligned}\dot{V} \le & -e_z^{\ T}\kappa_{11}e_z - \kappa_{12}\|e_z\| + \frac{5}{2}\|\Delta_e\|^2 - g_u\kappa_{21}e_u^{\ 2} - g_u\kappa_{22}\|e_u\| - \kappa_{11}e_\psi^{\ 2} - \kappa_{12}\|e_\psi\| \\ & - g_r\kappa_{21}e_r^{\ 2} - g_r\kappa_{22}\|e_r\| + \varsigma_{\max}\left(\kappa_{12}+\kappa_{22}\right) - \frac{\iota_1}{4g_u}\left(\Theta_u - g_u\hat{\Theta}_u\right)^2 - \frac{\iota_2}{4g_r}\left(\Theta_r - g_r\Theta_r\right)^2 \\ & - \frac{\iota_1}{2g_u}\left|\Theta_u - g_u\hat{\Theta}_u\right| - \frac{\iota_2}{2g_r}\left|\Theta_r - g_r\Theta_r\right| + \frac{\iota_1}{4g_u} + \frac{\iota_2}{4g_r} + \frac{\iota_1\Theta_u^{\ 2}}{2g_u} + \frac{\iota_2\Theta_r^{\ 2}}{2g_r} + \frac{\Theta_u}{4c_1} + \frac{\Theta_r}{4c_2} \\ & + \frac{1}{2}\left\|\Xi_u(t)m_u^{-1}\eta_u\right\|^2 + \frac{1}{2}\left\|\Xi_r(t)m_r^{-1}\eta_u\right\|^2 \\ \le & -\upsilon_1 V - \upsilon_2 V^{\frac{1}{2}} + \theta\end{aligned} \tag{32}$$

where $\upsilon_1 = \min\left\{2\kappa_{11}, 2g_u\kappa_{21}, 2g_r\kappa_{21}, \frac{\iota_1}{2}, \frac{\iota_2}{2}\right\}$,

$\rho_2 = \min\{\sqrt{2}\kappa_{12}, \sqrt{2}g_u\kappa_{22}, \sqrt{2}g_r\kappa_{22}, \frac{\iota_1}{\sqrt{2g_u}}, \frac{\iota_2}{\sqrt{2g_r}}\}$,

and

$$\begin{aligned}\theta = & \frac{\iota_1}{4g_u} + \frac{\iota_2}{4g_r} + \frac{\iota_1\Theta_u^{\ 2}}{2g_u} + \frac{\iota_2\Theta_r^{\ 2}}{2g_r} + \frac{\Theta_u}{4c_1} + \frac{\Theta_r}{4c_2} + \\ & + \varsigma_{\max}\left(\kappa_{12}+\kappa_{22}\right) + \frac{5}{2}\left\|\Delta_e\right\|^2 + \frac{1}{2}\left\|\Xi_u(t)m_u^{-1}\eta_u\right\|^2 + \frac{1}{2}\left\|\Xi_r(t)m_r^{-1}\eta_u\right\|^2\end{aligned}$$

Lemma 3: For the nonlinear system in Eq. (4), we assume that there exists a positive definite Lyapunov function $V(x)$: $\Omega_0 \to R$ and any scalar $a > 0$ $b > 0$, $0 < \kappa < 1$ such that the inequality $\dot{V}(x) + aV(x) + bV^{\kappa}(x) \le 0$ holds. The system in Eq. (4) is then finite time stable, and its regulation time meets the condition [37]:

$$T \le \frac{1}{a(1-t)}\ln\frac{aV^{1-\kappa}(x_0)+b}{b} \tag{33}$$

where $V(x_0)$ is the initial value of $V(x)$.

From Eq. (32), we obtain

$$\dot{V} \le -\phi\upsilon_1 V - (1-\phi)\upsilon_1 V - \upsilon_2 V^{\frac{1}{2}} + \theta \tag{34}$$

where $\phi = \min\{\phi_1, \phi_2\}$, $0 < \phi < 1$.

If $V > \frac{\upsilon}{\phi\upsilon_1}$, we obtain

$$\dot{V} \le -(1-\phi)\upsilon_1 V - \upsilon_2 V^{\frac{1}{2}} \tag{35}$$

According to Lemma 3, the system will stabilise in finite time to the region $\Omega_V = \left\{V : V \le \frac{\theta}{\phi\upsilon_1}\right\}$, and the stabilisation time is

$$T \le \frac{4}{(1-t)\upsilon_1}\ln\left[\frac{(1-t)\upsilon_1 V^{1/2}(0)+\upsilon_2}{\upsilon_2}\right] \tag{36}$$

From Eq. (19), the following expressions ,can be obtained:

$$\begin{cases} \dfrac{d}{dt}\left|e_{\xi_u}\right| = \dfrac{d}{dt}\left(e_{\xi_u} * e_{\xi_u}\right) \\ \qquad = sign\left(e_{\xi_u}\right)\dot{e}_{\xi_u} \le \left|\dot{\omega}_u\left(t\right)\right| \\ \dfrac{d}{dt}\left|e_{\xi_r}\right| = \dfrac{d}{dt}\left(e_{\xi_r} * e_{\xi_r}\right) \\ \qquad = sign\left(e_{\xi_r}\right)\dot{e}_{\xi_r} \le \left|\dot{\omega}_r\left(t\right)\right| \end{cases} \tag{37}$$

Furthermore, from Eq. (17), we know that

$$\begin{aligned} \dot{\omega}_u &= m_u\{-k_{21}\dot{e}_u - \frac{k_{22}\dot{e}_u}{\sqrt{\|e_u\|^2+\varsigma_u^2}} - [c_1\dot{e}_u\hat{\Theta}_u\zeta_u^{\ 2}(Z) + c_1e_u(\dot{\Theta}_u\zeta_u^{\ 2}(Z) + 2\Theta_u\zeta_u(Z)\dot{\zeta}_u(Z)] + \ddot{\alpha}_u\} \\ \dot{\omega}_r &= m_r\{-k_{41}\dot{e}_r - \frac{k_{42}\dot{e}_r}{\sqrt{\|e_r\|^2+\varsigma_r^2}} - [c_2\dot{e}_r\hat{\Theta}_r\zeta_r^{\ 2}(Z) + c_2e_r(\dot{\Theta}_r\zeta_r^{\ 2}(Z) + 2\Theta_r\zeta_r(Z)\dot{\zeta}_r(Z)] + \ddot{\alpha}_r\} \end{aligned} \tag{38}$$

From Eq. (39), $\dot{\omega}_i$, $i = u, r$ is a smooth and derivable function, and $\dot{\omega}_i$ is therefore a continuous function. Since all its variables are globally bounded, $\lambda_i > 0$ gives $\left|\dot{\omega}_i\right| \le \lambda_i$. When $t = t_k$, $e_{\xi_i}\left(t_k\right) = 0$ and $\lim\limits_{t\to t_k} e_{\xi_i}\left(t\right) = \eta_i$. Hence there exists a time interval t_k satisfying $t \ge \dfrac{\eta_i}{\lambda_i}$, and Zeno behavior does not occur.

SIMULATION

In this study, a Cybership 2 ship model from the Norwegian University of Science and Technology was used as the controlled object for simulation tests. The ship had a total length L = 1.255 m, a mass m = 23.8 kg, and other parameters as detailed in the literature [38].

Two different sets of equations, giving a circular and a trapezoidal trajectory, were used for the simulation, as shown in Eqs. (39) and (40).

The equations for the circular trajectory were as follows:

$$\begin{cases} x_d = 25\sin\left(0.01\pi t\right) \\ y_d = 25 - 25\cos\left(0.01\pi t\right) \end{cases} \tag{39}$$

The equations for the trapezoidal trajectory were:

$$\begin{cases} y_d = 10 & t \le 47 \\ y_d = \sqrt{100-\left(t-47\right)^2} & 47 < t \le 53 \\ y_d = \dfrac{65-t}{1.5} & 53 < t \le 62 \\ y_d = 10 - \sqrt{100-\left(t-68\right)^2} & 62 < t \le 68 \\ y_d = 0 & 68 < t \le 112 \\ y_d = 10 - \sqrt{100-\left(t-112\right)^2} & 112 < t \le 118 \\ y_d = \dfrac{t-115}{1.5} & 118 < t \le 127 \\ y_d = \sqrt{100-\left(t-133\right)^2} & 127 < t \le 133 \\ y_d = 10 & 133 < t \le 200 \end{cases} \tag{40}$$

To verify the effectiveness of the control scheme (ETC) proposed in this paper, two other approaches were selected for comparison:

Control scheme 1: Finite-time control scheme without event triggering (ANNs+FT) [39];

Control scheme 2: Adaptive control scheme using MLPs and ANNs (ANNs+MLPs) [40].

The virtual control rates, control rates, and adaptive laws for adaptive ANN trajectory tracking control using MLPs were as follows:

$$\begin{cases} \alpha_u = \left\| -k_{11}e_z - vg_v\left(e_\psi\right) + \begin{pmatrix} \dot{x}_d \\ \dot{y}_d \end{pmatrix} \right\| \\ \alpha_r = -k_{31}e_\psi + \dot{\psi}_d \end{cases} \tag{41}$$

$$\begin{cases} \tau_u = m_u\left[-k_{21}e_u - c_1e_u\hat{\Theta}_u\zeta_u^{\ 2}(Z) + \dot{\alpha}_u\right] \\ \tau_r = m_r\left[-k_{41}e_r - c_2e_r\hat{\Theta}_r\zeta_r^{\ 2}(Z) + \dot{\alpha}_r\right] \end{cases} \tag{42}$$

$$\begin{cases} \dot{\hat{\Theta}}_u = c_1\zeta_u^{\ 2}(Z)\left\|e_u\right\|^2 - \iota_1\hat{\Theta} \\ \dot{\hat{\Theta}}_r = c_2\zeta_r^{\ 2}(Z)\left\|e_r\right\|^2 - \iota_2\hat{\Theta} \end{cases} \tag{43}$$

To simulate the sea state, the first-order Markov equations in Eq. (44) were used to describe the environmental disturbance, as shown in Fig. 2. This approach can reflect the coupling between the high and low frequencies of the waves more realistically than using sinusoidal waves [38].

$$\begin{cases} \dot{d}_{wu} = -d_{wu} + 0.05 * \omega_u \\ \dot{d}_{wo} = -d_{wv} + 0.05 * \omega_v \\ \dot{d}_{wr} = -d_{wr} + 0.5 * \omega_r \end{cases} \tag{44}$$

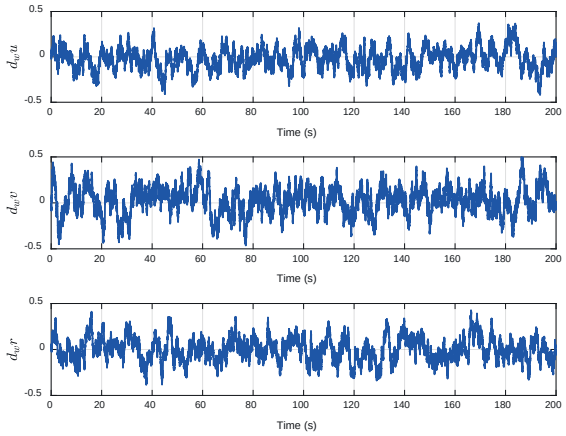

Fig. 2 Time evolution of the disturbances

In Fig. 2, $d_{wi} = d_i / m_i$, $i = \{u, v, r\}$ are three independent white noise variables with a variance of one.

Based on the condition that both model parameters m_u, m_v, m_r, $f_u(u,v,r)$ and $f_v(u,v,r)$ are unknown, we set the parameters $k_{11} = 0.3$, $k_{12} = 0.1$, $k_{21} = 0.2$, $k_{22} = 0.5$, $k_{31} = 3.5$, $k_{32} = 0.5$, $k_{41} = 2$, $k_{42} = 0.1$, $c_1 = 0.5$, $c_2 = 0.01$, $\iota_1 = 0.01$, $\iota_2 = 1$, $\varsigma_z = \varsigma_\psi = \varsigma_u = \varsigma_r = 0.05$, $\eta_u = 0.05$, $\eta_r = 0.5$. The initial position and velocity of the ship for the circular trajectory were $(x_0; y_0; \psi_0; u_0; v_0; r_0) = (0; 10; 0; 0; 0; 0)$. The initial position and velocity of the ship for the trapezoidal trajectory were $(x_0; y_0; \psi_0; u_0; v_0; r_0) = (3; 7; 75/57.3; 0; 0; 0)$.

The simulation results for the circular trajectory shown in Figs. 3–11 illustrate the tracking effect of the actual trajectory, and it can be seen that the three control schemes can track the target with good performance. Figs. 3–6 show the tracking of the ship's position, heading angle and speed. Figs. 2–6 show that the tracking effect of the system is greatly improved after the introduction of finite time and event triggering in the control scheme, and that there is no significant degradation in the control performance of the system after the introduction of event triggering. Figs. 7 and 8 show the ephemeral curves for the positional and velocity errors of the system. After introducing finite time to the control scheme, the convergence speed of the system errors is improved, and the upper and lower bounds on the errors are smaller. When event triggering is added, the tracking accuracy of the system is basically the same as that of the finite time control scheme. Fig. 9 shows the ephemeral curves for the control inputs of the system, and it can be seen that the number of updates to the control inputs of the event-triggered control scheme has been reduced. Fig. 10 shows the interval times between triggering events. In summary, the control performance of both control schemes proposed in this paper is greatly improved, and the number of updates to the controller is significantly reduced after the introduction of event triggering.

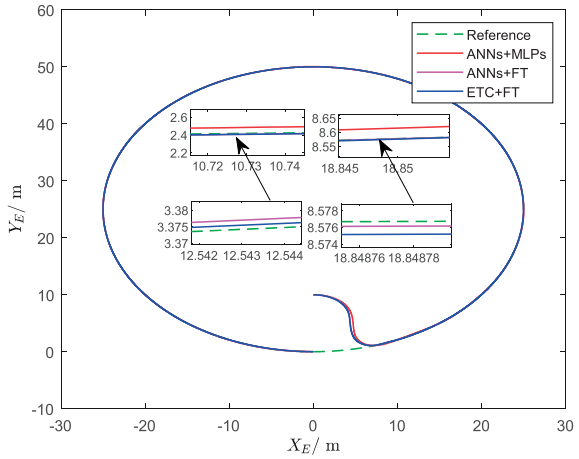

Fig. 3 Actual and reference trajectories in the (x, y) plane

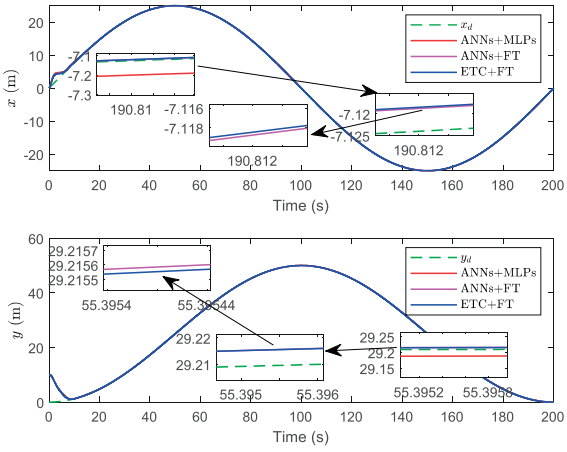

Fig. 4 Actual and reference positions

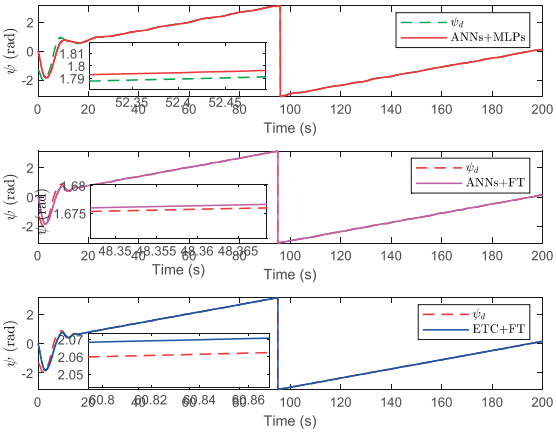

Fig. 5 Actual and reference yaw angles

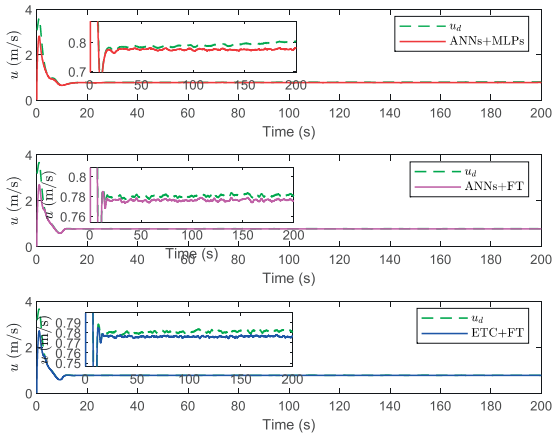

Fig .6 Surge velocity u

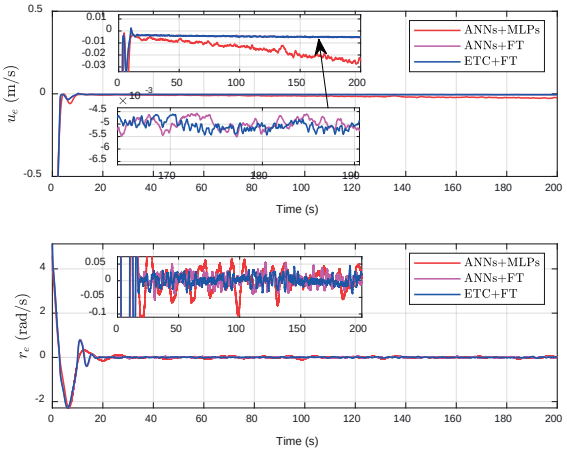

Fig. 9 Time evolution of the velocity errors

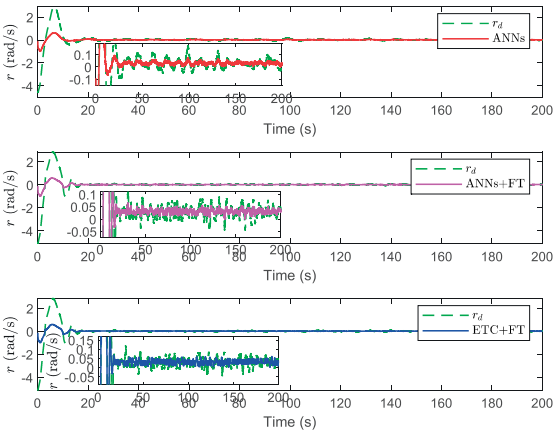

Fig.7 Yaw rate r

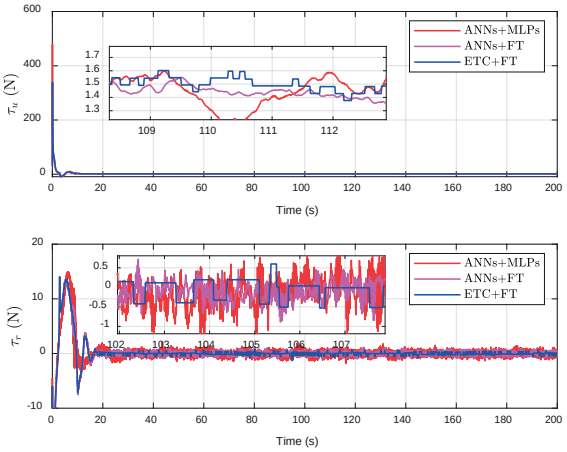

Fig. 10 Control input of τ_i *(* $i = u, r$ *)*

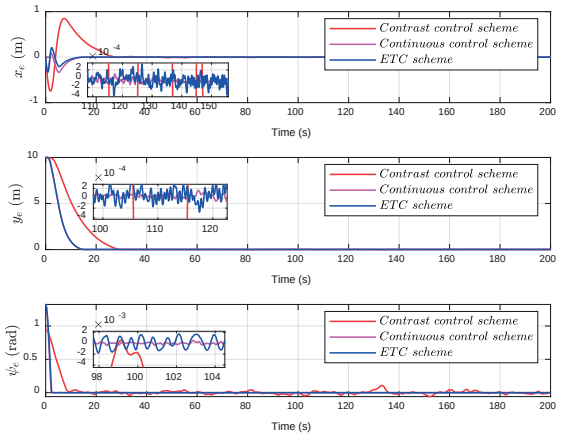

Fig. 8 Time evolution of the attitude errors

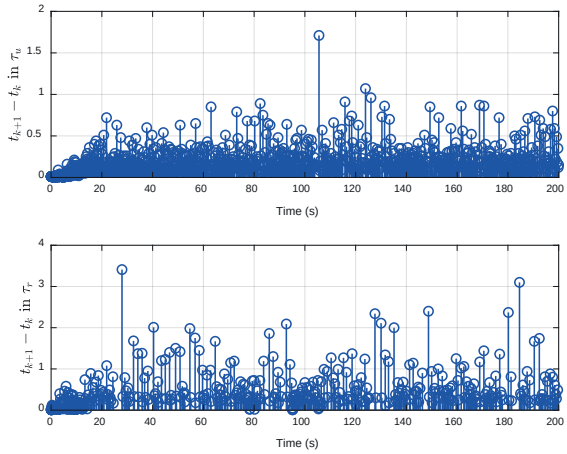

Fig. 11 Simulation of inter-event times

The simulation results for the trapezoidal trajectory are shown in Figs. 12–20. From the tracking effect and the error time curve, we see that the two control schemes proposed in this paper performed better than the control schemes without finite time and event triggering, and that the performance of the finite-time control scheme was not degraded when event triggering was added. As the trapezoidal trajectory was composed of multiple smaller trajectories, overshoot occurred at the points of trajectory switching. However, the tracking accuracy of the ET control scheme and the finite-time control scheme was better than for the non-ET and finite-time control schemes. Moreover, the results showed that the two control schemes presented in this paper could accomplish the task of tracking better under the condition of constant controller parameters. It is not difficult to see that the two control schemes designed in this paper have stronger robustness. As shown in Fig. 18, the ephemeral curves for the control inputs show that the number of controller updates was significantly reduced after the introduction of event triggering to the system.

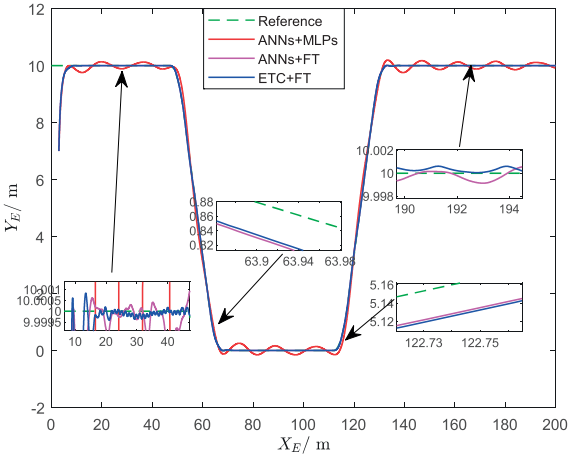

Fig. 12 Actual and reference trajectories in the $(x\ y)$ plane

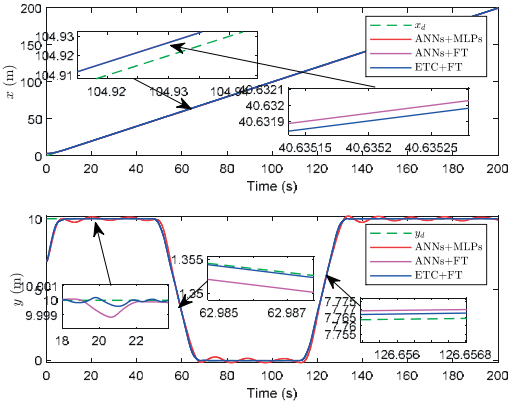

Fig. 13 Actual and reference positions

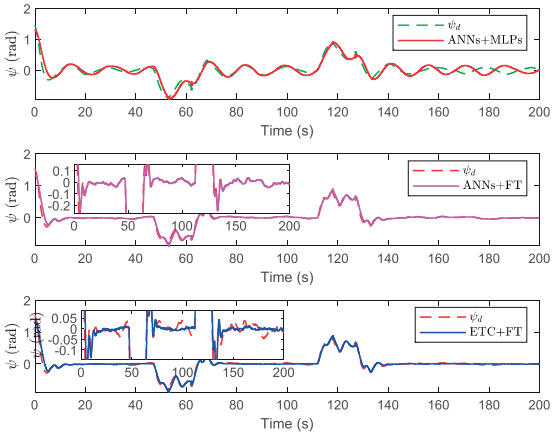

Fig. 14 Actual and reference yaw angles

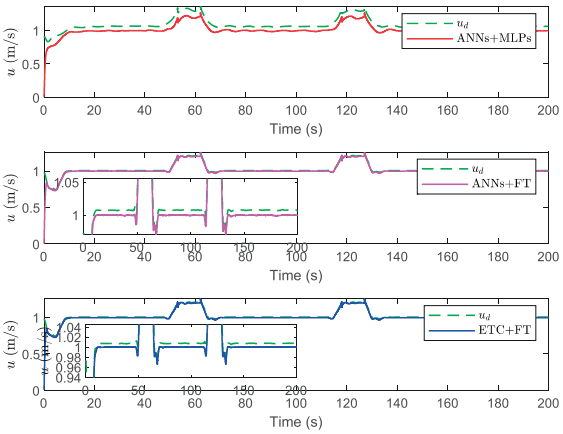

Fig. 15 Surge velocity u

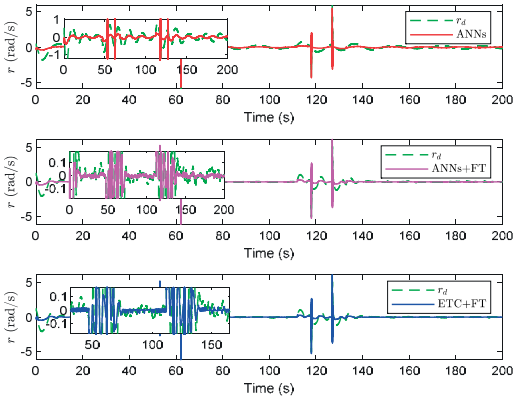

Fig. 16 Yaw rate r

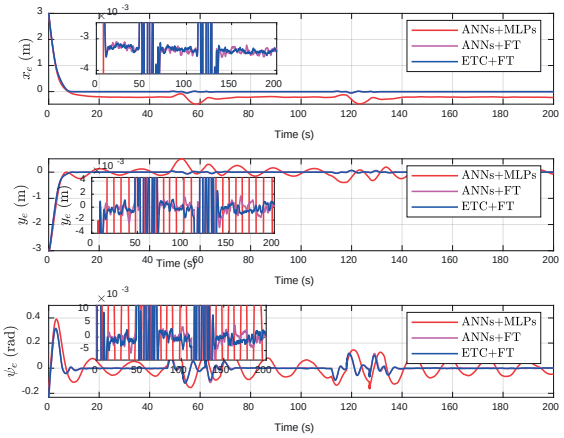

Fig. 17 Time evolution of the attitude errors

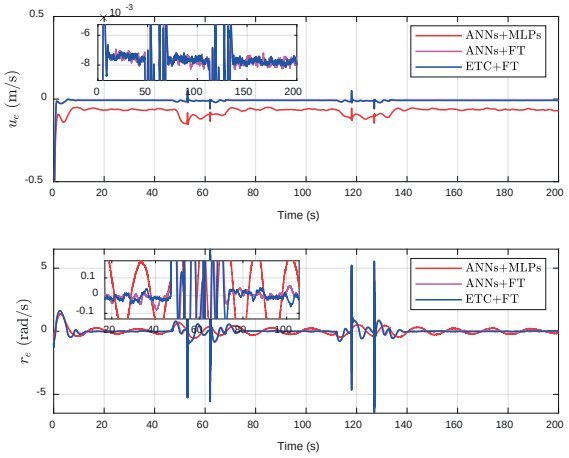

Fig. 18 Time evolution of the velocity errors

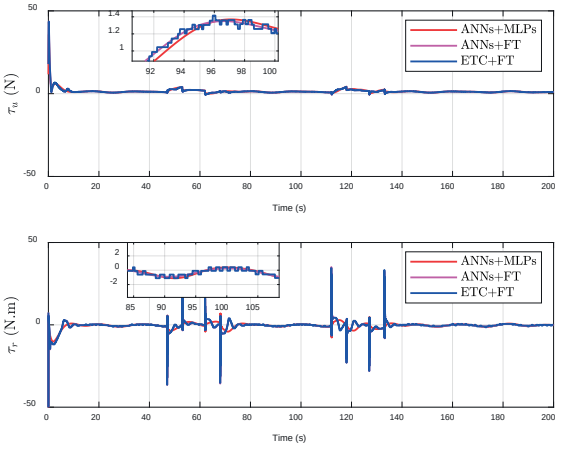

Fig. 19 Control input of τ_i ($i = u, r$)

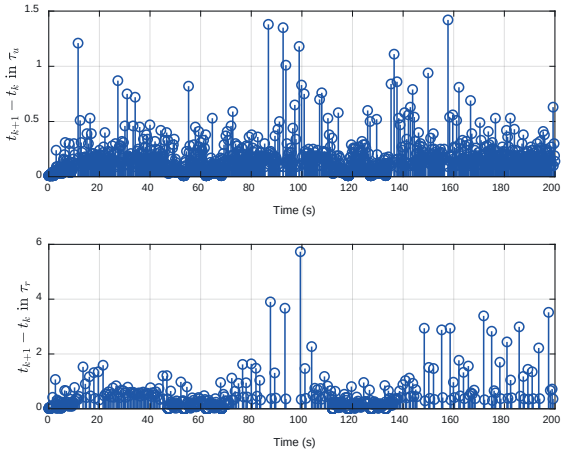

Fig. 20 Simulation of inter-event times

CONCLUSION

With the aim of tackling the problem of trajectory tracking for underactuated ships affected by internal and external uncertainties, this paper has presented an adaptive NN ET trajectory tracking control scheme for underactuated ships based on finite time convergence. The introduction of finite time was shown to greatly accelerate the convergence of system errors, and to further improve the tracking accuracy of the system. When combined with event triggering, the number of controller updates was also significantly reduced under the condition of ensuring the control accuracy of the system.

Compared with existing trajectory tracking control schemes, the controller structure of the control scheme in this paper is simpler and more suitable for engineering applications. However, the upper bound on the composite perturbation was approximated by an adaptive law with certain conservativeness, and the event trigger condition considered in this paper was essentially a static trigger. Further research is needed to design a more accurate perturbation compensation scheme and an event trigger condition that is more in line with engineering reality.

ACKNOWLEDGEMENTS

Sincere thanks are due to the Qingdao Harbor Vocation and Technology College Science and Technology Innovation Foundation No. QDGW2022Z02 and No. QDGW2020Z08.

REFERENCES

1. H. W. He, Z. J. Zou, and Z. H. Zeng, 'Adaptive neural network-sliding mode path following control for underactuated surface vessels,' Journal of Shanghai Jiaotong University, 2020, 54(09): 890-897, doi: 10.16183/j.cnki.jsjtu.2019.122.

2. H. Y. Xu, M. F. Zhu, W. Z. Yu, and X. Han, 'Robust adaptive control of automatic berthing for intelligent ships,' Journal of Huazhong University of Science and Technology (Natural Science Edition), 2020, 48(03): 25-29+40, doi: 10.13245/j.hust.200305.

3. N. Wang and H. R. Karimi, 'Successive waypoints tracking of an underactuated surface vehicle,' IEEE Transactions on Industrial Informatics, 2020, 16(2): 898-908, doi: 10.1109/TII.2019.2922823.

4. K. Jonghoek, 'Target following and close monitoring using an unmanned surface vehicle,' IEEE Transactions on Systems Man & Cybernetics Systems, 2020, 50(11): 4233-4242, doi: 10.1109/TSMC.2018.2846602.

5. G. Zhu, Y. Ma, and S. Hu, 'Single parameter learning based finite-time tracking control of underactuated MSVs under input saturation,' Control Engineering Practice, 2020, 105, doi: 10.1016/j.conengprac.2020.104652.

6. G. Zhu, Y. Ma, and Z. Li, 'Event-triggered adaptive neural fault-tolerant control of underactuated MSVs with input saturation,' IEEE Transactions on Intelligent Transportation Systems, 2021, PP (99): 1-13, doi: 10.1109/TITS.2021.3066461.

7. Y. Ma, G. Zhu, and Z. L, 'Error-driven-based nonlinear feedback recursive design for adaptive NN trajectory tracking control of surface ships with input saturation,' IEEE Intelligent Transportation Systems Magazine, 2019, PP (2): 1-1. doi:10.1109/MITS.2019.2903517.

8. C. J. Zhang, C. Wang, and W. Cao, 'Underactuated USV neural network adaptive trajectory tracking control,' Journal of Harbin Institute of Technology, 2020, 52(12): 7-13 doi: 10.11918/201905049.

9. W. J. Wang and J. Li, 'A direct adaptive sliding mode trajectory tracking control design based on an RBF neural network,' Machinery Design & Manufacture, 2020(11): 183-187, doi: 10.19356/j.cnki.1001-3997.2020.11.046.

10. N. Wang and H. He, 'Dynamics-level finite-time fuzzy monocular visual servo of an unmanned surface vehicle,' IEEE Transactions on Industrial Electronics, 2020, 67(11): 9648-9658, doi: 10.1109/TIE.2019.2952786.

11. Y. Cheng, Z. Sun, and Y Huang, 'Fuzzy categorical deep reinforcement learning of a defensive game for an unmanned surface vessel,' International Journal of Fuzzy Systems, 2019, 21(2): 592-606, doi: 10.1007/s40815-018-0586-0.

12. Y. Lu, 'Adaptive-fuzzy control compensation design for direct adaptive fuzzy control,' IEEE Transactions on Fuzzy Systems, 2018, 26(6): 3222-3231, doi: 10.1109/TFUZZ.2018.2815552.

13. N. Wang, Z. Sun, and J. Yin, 'Fuzzy unknown observer-based robust adaptive path following control of underactuated surface vehicles subject to multiple unknowns,' Ocean Engineering, 2019, 176: 57-64, doi: 10.1016/j.oceaneng.2019.02.017.

14. Y. Deng, X. Zhang, and N. Im, 'Adaptive fuzzy tracking control for underactuated surface vessels with unmodeled dynamics and input saturation,' ISA Transactions, 2020, 103, doi: 10.1016/j.isatra.2020.04.010.

15. D. Mu, G. Wang, and Y. Fan, 'Trajectory tracking control for underactuated unmanned surface vehicle subject to uncertain dynamics and input saturation,' Neural Computing and Applications, 2021, (6), doi: 10.1007/s00521-021-05922-x.

16. X. Zhang, 'Backstep sliding mode control for trajectory tracking of underactuated surface unmanned vehicles,' Digital Technology & Application, 2020, 38(01): 180-183, doi: CNKI:SUN:SZJT.0.2020-01-090.

17. S. Wang and Y. Tuo, 'Robust trajectory tracking control of underactuated surface vehicles with prescribed performance,' Polish Maritime Research, 2020, 27(4): 148-156, doi: 10.2478/pomr-2020-0075.

18. N. Wang, Y. Gao, and H. Zhao, 'Reinforcement learning-based optimal tracking control of an unknown unmanned surface vehicle,' IEEE Transactions on Neural Networks and Learning Systems, 2020, PP(99): 1-12, doi: 10.1109/TNNLS.2020.3009214.

19. B. Qiu, G. Wang, and Y. Fan, 'Path following of underactuated unmanned surface vehicle based on trajectory linearization control with input saturation and external disturbances,' International Journal of Control Automation and Systems, 2020, 18(4): 1-12, doi: 10.1007/s12555-019-0659-3.

20. Q. Zhang, Z. Ding, and M. Zhang, 'Adaptive self-regulation PID control of course-keeping for ships,' Polish Maritime Research, 2020, 27(1): 39-45, doi: 10.2478/pomr-2020-0004.

21. D. D. Wang, Q. Zong, and B. Y. Zhang, 'Fully distributed limited-time formation control of multiple UAVs,' Control

and Decision, 2019, 34(12): 154-158, doi: 10.13195/j.kzyjc.2018.0314.

22. N. Wang and C. K. Ahn, 'Hyperbolic-tangent LOS guidance-based finite-time path following of underactuated marine vehicles,' IEEE Transactions on Industrial Electronics, 2020, 67(10): 8566-8575, doi: 10.1109/TIE.2019.2947845.

23. M. Y. Hu, S. H. Yu, and Y. Y. Li. 'Finite time trajectory tracking control of ocean surface vessels based on command filtering with full state constraints,' Journal of Nanjing University of Science and Technology, 2021, 45(3): 10, doi: 10.14177/j.cnki.32-1397n.2021.45.03.003.

24. H. L. Chen, H. X. Ren, and B. C. Yang, 'Design of finite time controller for ship dynamic positioning based on LS-SVM,' Ship Engineering, 2020, 42(2): 8, doi: 10.13788/j.cnki.cbgc.2020.02.14.

25. P. Tabuada, 'Event-triggered real-time scheduling of stabilizing control tasks,' IEEE Transactions on Automatic Control, 2007, 52(9): 1680-1685, doi: 10.1109/TAC.2007.904277.

26. A. Girard, 'Dynamic triggering mechanisms for event-triggered control,' IEEE Transactions on Automatic Control, 2013, 60(7): 1992-1997, doi: 10.1109/TAC.2014.2366855.

27. W. Heemels and M. Donkers, 'Model-based periodic event-triggered control for linear systems,' Automatica, 2013, 49 (3): 698-711, doi: 10.1016/j.automatica.2012.11.025.

28. S. Gao, Z. Peng, and L. Liu, 'Coordinated target tracking by multiple unmanned surface vehicles with communication delays based on a distributed event-triggered extended state observer,' Ocean Engineering, 2021, 227(4): 108283, doi: 10.1016/j.oceaneng.2020.108283.

29. S. J. Yoo and B. S. Park, 'Guaranteed connectivity based distributed robust event-triggered tracking of multiple underactuated surface vessels with uncertain nonlinear dynamics,' Nonlinear Dynamics, 2020, 99(3): 2233-2249, doi: 10.1007/s11071-019-05432-5.

30. Y. Deng, X. Zhang, and N. Im, 'Model-based event-triggered tracking control of underactuated surface vessels with minimum learning parameters,' IEEE Transactions on Neural Networks and Learning Systems, 2020, 31(10): 1-14, doi: 10.1109/TNNLS.2019.2951709.

31. F. Wang, B. Chen, and X. Liu, 'Finite-time adaptive fuzzy tracking control design for nonlinear systems,' IEEE Transactions on Fuzzy Systems, 2017, 26(3), 1207-1216, doi: 10.1109/TFUZZ.2017.2717804.

32. W. T. Wu, N. Gu, and Z. H. Peng, 'Distributed time-varying formation control of multi-pilot guided unmanned ship swarms,' Chinese Journal of Ship Research, 2020, 15(01): 21-30, doi: 10.19693/j.issn.1673-3185.01734.

33. Q. Zhang, G. Zhu, and X. Hu, 'Adaptive neural network auto-berthing control of marine ships,' Ocean Engineering, 2019, 177(APR.1): 40-48, doi: 10.1016/j.oceaneng.2019.02.031.

34. B. Xu and Y. Shou, 'Composite learning control of MIMO systems with applications,' IEEE Transactions on Industrial Electronics, 2018, PP(99):1-1, doi: 10.1109/TIE.2018.2793207.

35. M. Li, T. Li, and X. Gao, 'Adaptive NN event-triggered control for path following of underactuated vessels with finite-time convergence,' Neurocomputing, 2020, 379(Feb.28): 203-213, doi: 10.1016/j.neucom.2019.10.044.

36. Q. Zhang, M. Zhang, and R. Yang, 'Adaptive neural finite-time trajectory tracking control of MSVs subject to uncertainties,' International Journal of Control Automation and Systems, 2021, 19(6): 2238-2250, doi: 10.1007/s12555-020-0130-5.

37. Y. Huang and Y. Jia, 'Adaptive fixed-time six-DOF tracking control for noncooperative spacecraft fly-around mission,' IEEE Transactions on Control Systems Technology, 2019, 27(4): 1-9, doi: 10.1109/TCST.2018.2812758.

38. R. Skjetne, T. I. Fossen, and P. V. Kokotovi, 'Adaptive maneuvering, with experiments, for a model ship in a marine control laboratory,' Pergamon Press, Inc. 2005, 41(2): 289-298.

39. C. Y. Wu, L. L. Fan, and H. H. Ji, 'Finite-time consensus control by using adaptive neural networks control,' Engineering of China, 2022, 29(03): 455-463, doi: 10.14107/j.cnki.kzgc.20210489.

40. Q. Zhang, Y. C. Hu, and A. Q. Wang, 'Nonlinear adaptive control algorithm based on dynamic surface control and neural networks for ship course-keeping controller,' Journal of Applied Science and Engineering, 2017, 20(2): 157-163, doi: 10.6180/jase.2017.20.2.03.